December 31, 2017, Revised 7 May 2018

What Fraction of the Pacific and Indian Oceans' Deep Water is formed in the Southern Ocean?

James W.B. Rae
School of Earth & Environmental Sciences
Irvine Building
University of St. Andrews
St. Andrews
KY16 9AL
UK
jwbr@st-andrews.ac.uk

Wally Broecker
Lamont-Doherty Earth Observatory of Columbia University
61 Route 9W/PO Box 1000
Palisades, NY 10964
broecker@ldeo.columbia.edu; (845) 365-8413 tel; (845) 365-8169 fax

Contribution to the
Ernst Maier-Reimer Volume

Abstract

In this contribution we explore constraints on the fractions of deep water present in Indian and Pacific Oceans which originated in the northern Atlantic and in the Southern Ocean. Based on PO_4^* we show that if ventilated Antarctic shelf waters characterize the Southern contribution, then the proportions could be close to 50-50. If instead a Southern Ocean bottom water value is used, the Southern contribution is increased to 75 %. While this larger estimate may best characterize the volume of water entering the Indo-Pacific from the Southern Ocean, it contains a significant portion of entrained northern water. We also note that ventilation may be highly tracer dependent: for instance Southern Ocean waters may contribute only 35% of the deep radiocarbon budget, even if their volumetric contribution is 75%. In our estimation, the most promising approaches involve using CFC-11 to constrain the amount of deep water formed in the Southern Ocean. Finally, we highlight the broad utility of PO_4^* as a tracer of deep water masses, including descending plumes of Antarctic Bottom Water and large-scale patterns of deep ocean mixing, and as a tracer of the efficiency of the biological pump.

Remembering Ernst (W.B.)

In 1987, Klaus Hasselmann was invited to Lamont-Doherty to present three lectures on climate. The first two dealt with what he referred to as PIPS and POPS. They didn't ring my bell. But the third one hit home. In it Klaus laid out the distribution of properties generated by Ernst Maier-Reimer's ocean circulation model (Maier-Reimer & Hasselmann, 1987). I was particularly interested in its ability to reproduce the distribution of natural radiocarbon in the ocean. But the plots he showed were at first look incomprehensible. It turned out, that rather than presenting differences from the ^{14}C to C ratio in atmospheric CO_2, they were referenced to that in mean ocean water. After the lecture, I offered to come to Hamburg to help Maier-Reimer switch to a mode of presentation understandable to those conversant with the ^{14}C measurements. And so it was I spent three weeks with Ernst probing not only the ^{14}C to C distribution produced by his model, but also that of O_2 and SiO_2. For me it was a fantastic learning experience. Not only did Ernst have an amazing mind but he had a knack of teaching by tweaking his model. Thus began a lasting collaboration and friendship.

PO_4^*

This led to an interest in determining the contributions of NADW and AABW to the ventilation of the deep Pacific and Indian Oceans. As the ratio of O_2 utilization to PO_4 release during respiration appears to be nearly constant throughout the ocean's interior (Takahashi et al. 1985; Anderson & Sarmiento, 1994), Broecker and colleagues (Broecker et al., 1985, Broecker et al., 1998) proposed a conservative property PO_4^*:

$$PO_4^* = PO_4 + \frac{O_2}{175} - 1.95\ \mu mol/kg.$$

As only differences between PO_4^* values are of importance, the choice of the constant 1.95 is arbitrary. Hence zero would have been more convenient. Other choices for the O_2 consumption to PO_4 remineralisation ratio are also possible (Hupe & Karstensen, 2000), but have little impact

on our global-scale calculations, so we stick with the formulation of Broecker et al. (1998) above.

The attraction of PO_4^* as a water mass tracer is that although the deep waters formed in the northern Atlantic range widely in temperature, all the contributors have PO_4^* values close to 0.7 (Figure 1). Further, the deep waters (i.e., >2000 m) in the deep Pacific and Indian Oceans have PO_4^* values close to 1.4. Hence were the PO_4^* for deep waters formed in the Southern Ocean known, the relative amounts of deep water produced in the two key source regions could be established.

Based on PO_4^*, Broecker et al. (1998) concluded that the deep Pacific and Indian Oceans received about half of their water from the northern Atlantic and half from the Southern Ocean. However, Johnson (2008), Gebbie & Huybers (2010), Primeau & DeVries (2011), and Khatiwala et al. (2012), using more complex inversions of multiple tracers and model-data synthesis, concluded that only about one quarter of this water came from the northern Atlantic.

Here we attempt to resolve this discrepancy by re-examining the PO_4^*-based approach. We show that much of the mismatch may be resolved by consideration of what "counts" as Southern-sourced water. Crucial to this discussion is the extent to which deep waters acquire their tracer signatures by ventilation in the surface ocean or by entrainment during descent. Our discussion is focussed on the volumetric contribution of Northern and Southern water masses to the deep Indo-Pacific, rather than water fluxes. Flux information – for tracers or for parcels of water – must be informed by estimates of residence time or formation rates, and we briefly discuss the potential of radiocarbon and CFCs to provide such information.

PO_4^* calculations revisited

Based on the GLODAPv2 dataset (Key et al., 2015; Olsen et al., 2016) we have re-examined deep ocean PO_4* distributions. The mean PO_4* value for deep (>2000 m) Indo-Pacific waters (Figure 2) is 1.42 ±0.04 (1 SD). We select waters below 2000 m as all determinations (Johnson, 2008; Gebbie and Huybers, 2010; Khatiwala et al., 2012) suggest that these depths are

predominantly a two-component mixture of deep North Atlantic and Southern Ocean waters. To help identify recently ventilated dense waters we also examined CFC11 and neutral density. The mean PO_4* value for deep (>1500 m) recently ventilated (CFC11>0.5 pmol/kg) waters in the North Atlantic (Figure 2) is 0.74 ±0.05. These Indo-Pacific and Atlantic end-members are within error of Broecker et al. (1998)'s values (1.39 and 0.73 respectively) and are relatively insensitive to choice of geographical boundaries, depth, CFC, and density limits.

Determining the PO_4* end member of Southern Ocean deep waters is less straightforward. Broecker et al. (1998) use a PO_4^* value of 1.95. This value was obtained both by extrapolating the PO_4^* - Θ relationship to the freezing point of sea water (Figure 1) and from direct observations of sinking surface waters in the Weddell and Ross Seas (Figure 3). The 1.95 PO_4^* value is achieved if water upwelling in the Southern Ocean is cooled to the freezing point, has about 65 percent of its O_2 deficiency replenished, and loses little of its PO_4 to sinking organics (see Table 1).

However while PO_4* values of 1.95 characterize well-ventilated Antarctic shelf waters, these entrain up to three times their volume in circumpolar deep water as they cascade down the continental slope (Carmack & Foster, 1975; Orsi et al., 1999); indeed PO_4* beautifully highlights this process (Figure 3). As a result, by the time Antarctic bottom water enters the ACC it has much lower PO_4*: Weddell Sea bottom waters have PO_4* of ~1.8, and deep Ross Sea waters ~1.6 (Figures 3 & 4). This basinal difference may be attributed to less input of NADW-influenced circumpolar deep water and higher local ventilation rates in the Weddell Sea, elevating PO_4* in this more enclosed basin. The average circumpolar PO_4* for recently ventilated (CFC-11 >0.5 pmol/kg) waters that have made it off the Antarctic shelf (>1500 m) and have neutral density higher than any North Atlantic waters (>28.3 kg/m^3) is 1.64 ±0.07 (1 SD; Figures 4 & 5).

Repeating Broecker et al.'s PO_4* mass balance calculation with the Southern Ocean bottom water value of 1.65 suggests that the deep Indo-Pacific is filled by 75 % Southern-sourced water and 25 % NADW, with an uncertainty of ± 9% (1 SD). This is within error of the

values obtained by Johnson (2008), Gebbie and Huybers (2010) and Khatiwala et al. (2012). However if we use the well-ventilated shelf water value of 1.95, the north-south balance is closer to 50-50 (Broecker et al. 1998). This highlights that while the volume of what are typically considered southern deep waters in the Indo-Pacific may substantially outweigh that of NADW, much of this water is entrained in the subsurface and does not reflect full Southern Ocean ventilation. Note that while sinking waters in the North Atlantic also entrain surrounding waters on descent, these are of recent northern origin. Entrainment in the North Atlantic thus does not substantially influence the PO_4^* signature of NADW nor the inference that this water is fully ventilated in the North Atlantic.

Differences in the extent to which the Southern Ocean end member is locally ventilated may thus explain much of the difference between the north-south balance obtained by Broecker et al. (1998) versus Johnson (2008), Gebbie & Huybers (2010), and Khatiwala et al. (2010). Johnson (2008) uses bottom water end member values for AABW, so it is unsurprising that our estimates using a Southern Ocean bottom water value are similar to his. Gebbie & Huybers (2008) and Khatiwala et al. (2010) use surface mixed layer conditions south of the ACC (Orsi et al., 1995), taken from gridded climatologies (WOA, Conkright et al., 1994; WOCE, Gouretski & Koltermann, 2004). As discussed by Gebbie & Huybers (2010), gridded data struggles to capture shelf features and dense overflow waters, and may thus miss some of the end member values characteristic of the ventilated Southern Ocean interior (Warren 1981). More crucially, high adiabatic upwelling rates (Toggweiler & Samuels, 1995; Marshall & Speer, 2012) and deep mixed layers (Gordon & Huber 1990; Dong et al., 2008) may also lead to inclusion of upwelled northern waters in these Southern end members, despite little property modification in the Southern Ocean surface. These issues may explain why the southern proportions of Gebbie & Huybers (2008) and Khatiwala et al. (2010) are larger than those using the ventilated PO_4* end member (as in Broecker et al., 1998) and lie close to our estimates using bottom water PO_4* values.

Note that we do not wish to imply that Antarctic shelf water is necessarily the most appropriate or only component to characterise ventilated Southern Ocean waters. As pointed out by Johnson (2008), shelf waters may have too unique a set of tracer properties to usefully capture the range of Southern Ocean water mass characteristics mixed into the deep Indo-Pacific. Furthermore while a 50-50 mixture between NADW and Antarctic shelf waters can produce the PO_4^* signature of deep Indo-Pacific waters, it gives too high a salinity, so more Southern-sourced water is required. Processes besides shelf water formation may also help ventilate deep Southern-sourced waters, such as deep winter mixing in the open Southern Ocean (Gordon & Huber, 1990; Dong, 2008) and exchange along steeply dipping isopycnals in the Antarctic Circumpolar Current (Abernathy & Ferreira, 2015).

The key issue that we aim to bring awareness to is discussion of what "counts" as ventilated Southern water. Implicit in the Gebbie & Huybers (2008) and Khatiwala et al. (2010) studies is that any waters reaching the Southern Ocean mixed layer may be considered Southern Ocean waters. However these waters may experience little equilibration with Antarctic surface conditions, including cooling, gas exchange, and nutrient use, depending on their transit time through the Southern Ocean surface and the relaxation time of the tracer of interest. Therefore while they may count in the inventory of water volume entering the deep Indo-Pacific from the Southern Ocean (Talley 2013; Marshall & Speer 2012; Lumpkin & Speer 2007), they may only partially reflect the exchanges of heat and CO_2 key to the Southern Ocean's role in climate (Stocker & Johnsen 2003; Marinov et al., 2006; Barker et al., 2009; Sigman et al., 2010; Ferrari et al. 2014).

Ventilation and the Radiocarbon Budget

The difference between Southern Ocean water mass volume and tracer ventilation is particularly pronounced in the deep radiocarbon budget. Of the 220 moles per year of ^{14}C undergoing radiodecay in the deep sea, about 20 moles/yr are resupplied by particle rain. As NADW supplies about 130 moles ^{14}C/yr, this leaves about 70 to be supplied from the Southern

Ocean (see Table 2). Ventilation of radiocarbon is thus dominated by the North Atlantic, even if the Southern Ocean contributes greater volume. This is due to ^{14}C's long equilibration time and the limited exchange time between Southern Ocean surface waters and the atmosphere. Waters upwelled into the Southern Ocean surface thus do not reach equilibrium for ^{14}C and radiocarbon gradients between surface and deep waters are very small (Broecker et al. 1985). This, along with the presence of ^{14}C produced by H-bomb testing, also introduces large uncertainty into any attempt to use radiocarbon to quantify the contribution of Southern Ocean waters to the deep Indo-Pacific. The importance of northern versus southern ventilation may thus depend on the tracer and process of interest.

Constraints Based on CFCs

Further insights into Southern Ocean ventilation may be obtained using CFC data, which also offer the potential to constrain flux information. As with ^{14}C, the degree of surface water saturation (Schlosser et al., 1991) must be carefully considered if the input flux of CFC tracer is to be converted to a ventilation flux for southern ocean water volume (England et al., 1994). However CFCs have the advantages over ^{14}C of a much larger surface to deep gradient and faster and less complicated equilibration. CFC-based estimates of the flux of ventilated Southern Ocean water give values of ~15 Sv (Orsi et al., 2002; Schlitzer 2007). This is similar to values for net production of NADW (Broecker et al., 1998; Ganachaud & Wunsch, 2000; Smethie & Fine, 2001), so appears to support roughly equal ventilation of the deep ocean by the northern Atlantic and the Southern Ocean (Broecker et al., 1998; Peacock et al., 2000; Orsi et al., 2001). However this does not rule out a much higher water flux from the south (Sloyan & Rintoul, 2001; Lumpkin & Speer, 2007; Talley 2013) – just not full equilibrium with Southern Ocean surface conditions. Furthermore some of the ~16 Sv of NADW may be lost to mixing or entrainment into Antarctic Intermediate or Bottom Waters (Primeau & Holzer, 2006), so the ventilation flux into the deep Indo-Pacific is likely still weighted towards the South. We also note that if diffusion down isopycnals in the open Southern Ocean is an important contributor to

regional ventilation (Abernathy & Ferreira, 2015), this may not be as easily picked up as the CFC signal in shelf waters (Figure 5). The reason is that low CFC-11 concentrations in a large volume may match high CFC-11 concentrations in a small volume. Finally, even if the fluxes of Northern and Southern sourced waters into the deep Indo-Pacific are similar, it is possible for Southern-sourced waters to form a larger volumetric contribution if they have a longer residence time (Johnson 2008), which is quite plausible given their injection onto deeper density surfaces.

PO_4^* and other tracers of the global overturning circulation

The large dynamic range of PO_4^* in the deep ocean makes it an effective tracer of the large scale circulation and mixing processes that make up the global overturning circulation. Its utility is highlighted by the PO_4^* sections, surfaces, and tracer-tracer plots in Figures 6-8, Supplementary Figures A1-6, and the SOCCOM data product (Verdy & Mazloff, 2017). As can be seen, low PO_4^* water from the North Atlantic mixes with high PO_4^* water formed in the Southern Ocean. This mixing occurs along shared isopycnals in the ACC (Figure 7; Abernathy & Ferreira, 2015), over rough seafloor topography (Naveira Garabato et al., 2004; Roemmich et al., 2009), and in the deep surface mixed layer of the Southern Ocean (Gordon & Huber 1990; Dong et al., 2008). These mixing patterns are also well illustrated on cross plots of PO_4^* with salinity and potential temperature (Figures 8 and A1-3). NADW is identifiable as a salinity and PO_4^* maximum sandwiched between fresher and higher PO_4^* southern waters above and below. Mixing between these Northern and Southern waters is well-illustrated by the linear trends in the PO_4^*-salinity plot (Figure 8). By the time circumpolar deep waters reach the Drake Passage, they have been somewhat homogenised, though a PO_4^* minimum at mid-depths remains, tracing the persistent influence of North Atlantic waters (Figure 6).

Other features of interest that are well highlighted by PO_4^* include: the input of very low PO_4^* deep water from the Mediterranean Sea into mid-depths of the North Atlantic (Figure 7 & A4); the penetration of relatively high PO_4^* water with a strong southern influence into the deep NE Atlantic (Figure 7, A1, A6); and the formation of mid-depth circumpolar deep waters

represented by a PO_4^* maxima, slightly underlying the salinity minimum of AAIW. Intermediate waters themselves are less readily identified by PO_4^*, forming in frontal regions with large nutrient gradients (Talley, 1993; Talley, 1996; Sarmiento et al., 2004), and are better traced by salinity (Figures 8, A1-3). Pacific deep waters returning through the Drake Passage are also hard to identify using PO_4^*, falling in the middle of a PO_4^* mixing gradient between northern and southern waters (Figure 7), and are better identified by their low oxygen and high silicate (Figures A3, A5, A6).

Alongside its use as a water mass tracer, PO_4^* may also provide complementary information on the carbon cycle. High PO_4^* waters, such as those found in the Southern Ocean, are subducted with high preformed phosphate and high oxygen; this indicates inefficient operation of the biological carbon pump and extensive ocean-atmosphere gas exchange, allowing net loss of CO_2 from the ocean to the atmosphere. PO_4^* is close in formulation to preformed phosphate (Ito & Follows, 2005), but differs in not accounting for changes in oxygen uptake as a function of temperature and salinity, and making no assumption of initial oxygen saturation. Nonetheless, the ease with which PO_4^* can be calculated makes it a useful qualitative measure of the carbon cycle in the surface ocean, complementing its more quantitative use as a conservative water mass tracer at depth.

Conclusions

The use of PO_4^* to constrain the northern and southern contributions to the waters in the deep Indian and Pacific Oceans is highly dependent on the Southern Ocean end member value. Using end members characterizing ventilated Antarctic shelf waters versus Southern Ocean deep waters brackets the southern contribution to between 50 and 75 % respectively. There is value to both of these estimates: 75-25 may best characterize the ratio of deep Southern Ocean to North Atlantic water volume, while 50-50 may better represent the ratio of well-ventilated waters. In other words a large volume of the ocean's water experiences some degree of exposure to the

Southern Ocean surface, but the volume of those taking on a more completely ventilated Southern Ocean signal is much smaller.

Acknowledgments

We thank Jake Gebbie and Jean Lynch-Steiglitz for their thoughtful reviews, and Jake Gebbie, Greg Johnson, and Jess Adkins for helpful discussions, all of which substantially improved this manuscript. We also thank Matthew Mazloff for making PO_4^* available as part of the B-SOSE product (http://sose.ucsd.edu/BSOSE_iter105_solution.html). W.B. acknowledges funding from the Comer Science and Education Foundation. mJ.W.B.R. acknowledges funding from NERC standard grants NE/N003861/1 and NE/N011716/1, and support from the School of Earth and Environmental Sciences at the University of St Andrews during W.B.'s visit, which sparked the discussions that led to this paper.

Table 1. Expected PO_4^*

Upwelled PO_4 = 2.2 µmol/kg

Upwelled O_2 = 210 µmol/kg

Saturation O_2 = 360 µmol/kg

Assume

1) No PO_4 utilization
2) 65% O_2 resaturation

Then

$$PO_4^* = 2.2 + \frac{0.65\ (360-210)+210}{175} - 1.95 = 1.95\ \mu mol/kg$$

Table 2. Example ^{14}C budget for ~25% NADW contribution.

Loss via Radiodecay	
Volume of deep sea	$8 \times 10^{17} m^3$
Mean ΣCO_2	2.3 moles/m^3
Mean $\Delta^{14}C$	-175‰
Mean $^{14}C/C$	1.0×10^{-12}
Amount of ^{14}C in deep sea	1.8×10^6 moles
Amount decaying	220 moles/yr
Gain of Radiocarbon from North Atlantic	
Flux	16 Sverdrups
Flux	$6 \times 10^{14} m^3$/yr
ΣCO_2	2.1 moles/m^3
$\Delta^{14}C$	-67‰
$^{14}C/C$-$^{14}C/C$ mean deep sea	0.13×10^{-12}
Input ^{14}C to deep sea	130 moles/yr
Gain of Radiocarbon from Southern Ocean	
Flux	45 Sverdrups
Flux	$17 \times 10^{14} m^3$yr
ΣCO_2	2.2 moles/yr
$\Delta^{14}C$	-154‰
$^{14}C/C$-$^{14}C/C$ mean deep sea	0.025×10^{-12}
Input ^{14}C to deep sea	70 moles/yr
Gain of Radiocarbon by Particle Flux	
Carbon flux	0.5 moles/m^2yr
$\Delta^{14}C$	-70‰
$^{14}C/C$-$^{14}C/C$ mean deep sea	0.126×10^{-12}
Input ^{14}C to deep sea	20 moles/yr
Total Gain of Radiocarbon	220 moles/yr

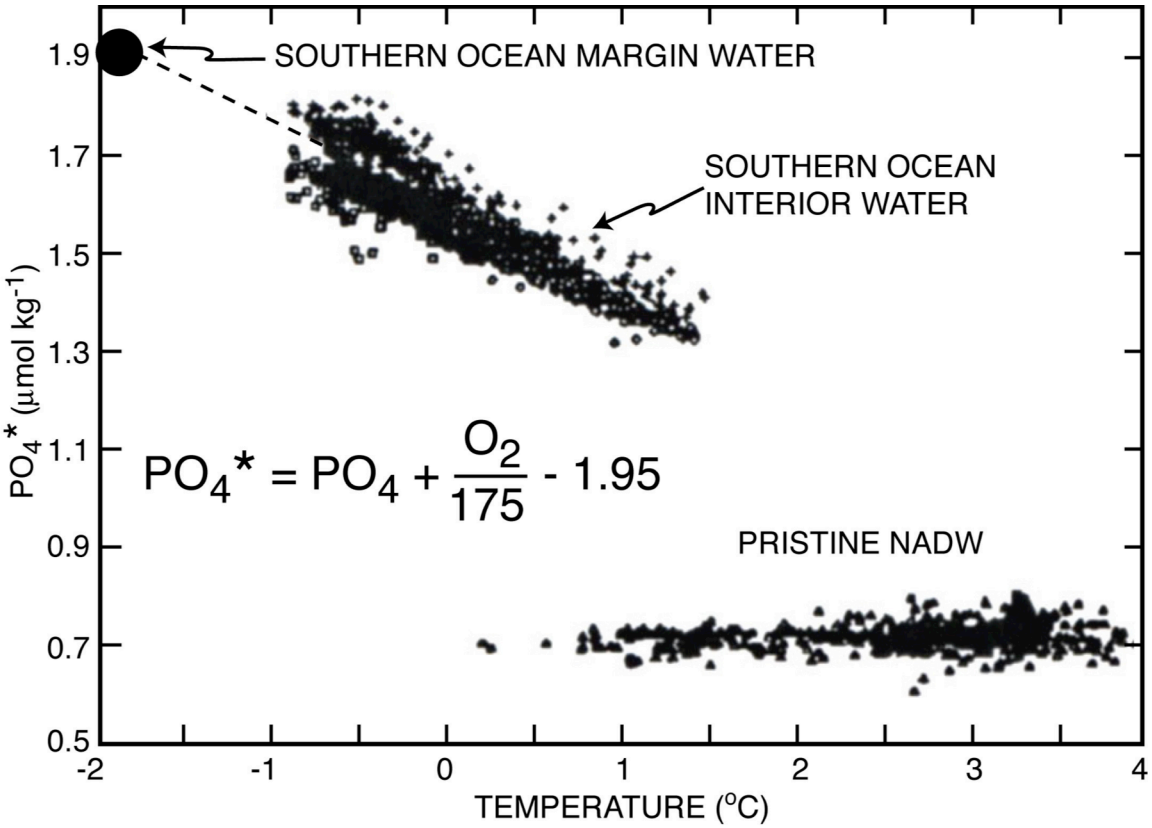

Figure 1. Plots of PO_4^* versus potential temperature for water formed in the northern Atlantic and in the Southern Ocean (based on measurements made as part of the GEOSECS expeditions). Note that all contributors of NADW have PO_4^* values within the measurement error of 0.75 µmol/kg. The Southern Ocean PO_4^* was originally obtained by extrapolating the observed PO_4^* - temperature trend to sea water's freezing point (Table 1). As shown in Figures 3 and 4, this extrapolated value is consistent with values observed close to the Antarctic margin in the Weddell Sea.

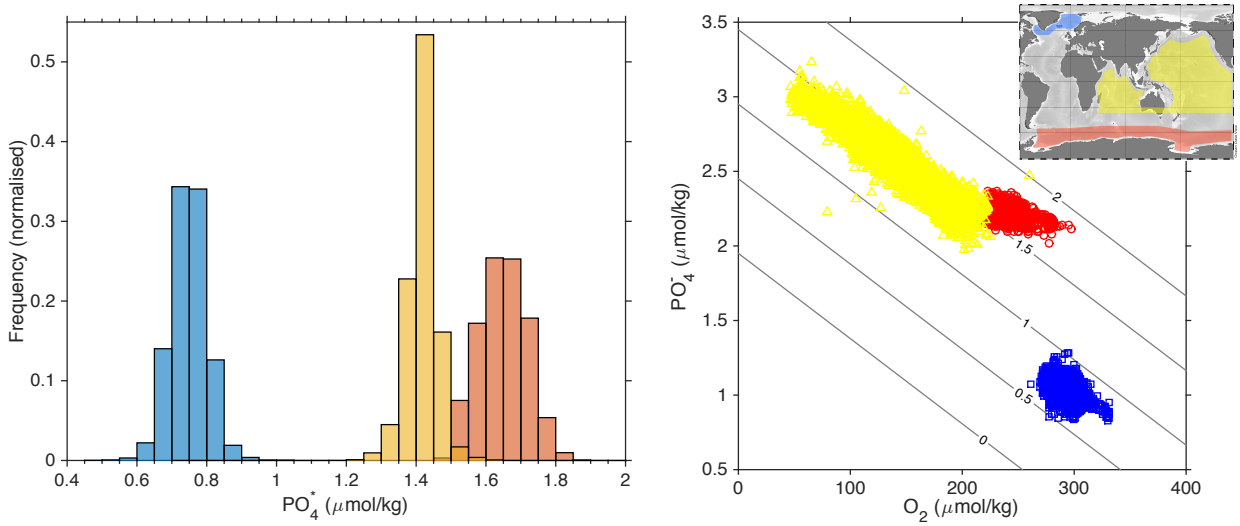

Figure 2: End member PO_4^* values for deep North Atlantic waters (blue) and deep Southern Ocean waters (red), along with deep Indo-Pacific waters (yellow). Data are from GLODAPv2 (Key et al., 2015; Olsen et al., 2016) and taken from the regions shown in the inset map. North Atlantic data are >1500 m and have CFC11>0.5 pmol/kg; Southern Ocean data are >1500 m, have CFC11>0.5 pmol/kg, and neutral density >28.3 kg/m^3 (see Figure 4); Indo-Pacific data are >2000 m. Normalised histograms of PO_4^* are shown for each region in the left hand panel, and the corresponding O_2 and PO_4 concentrations on the right, contoured with PO_4^*.

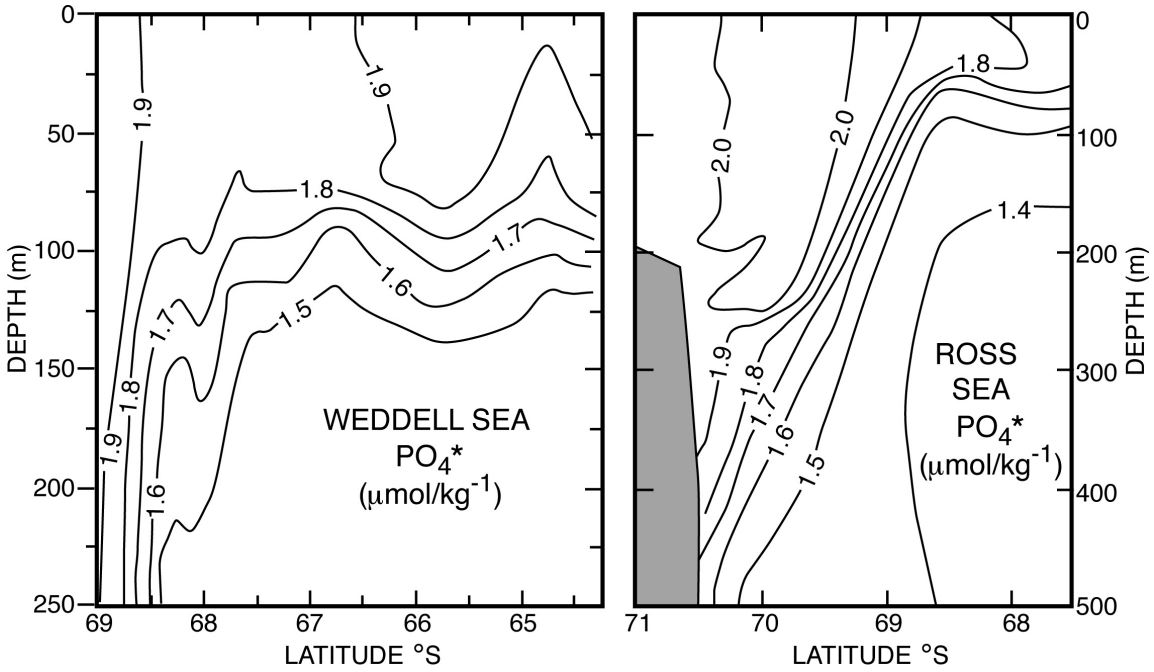

Figure 3. PO_4^* sections extending out from the Antarctic continent for the Weddell and Ross Seas. As can be seen, water with a value close to 1.95 is descending in a narrow margin-hugging plume.

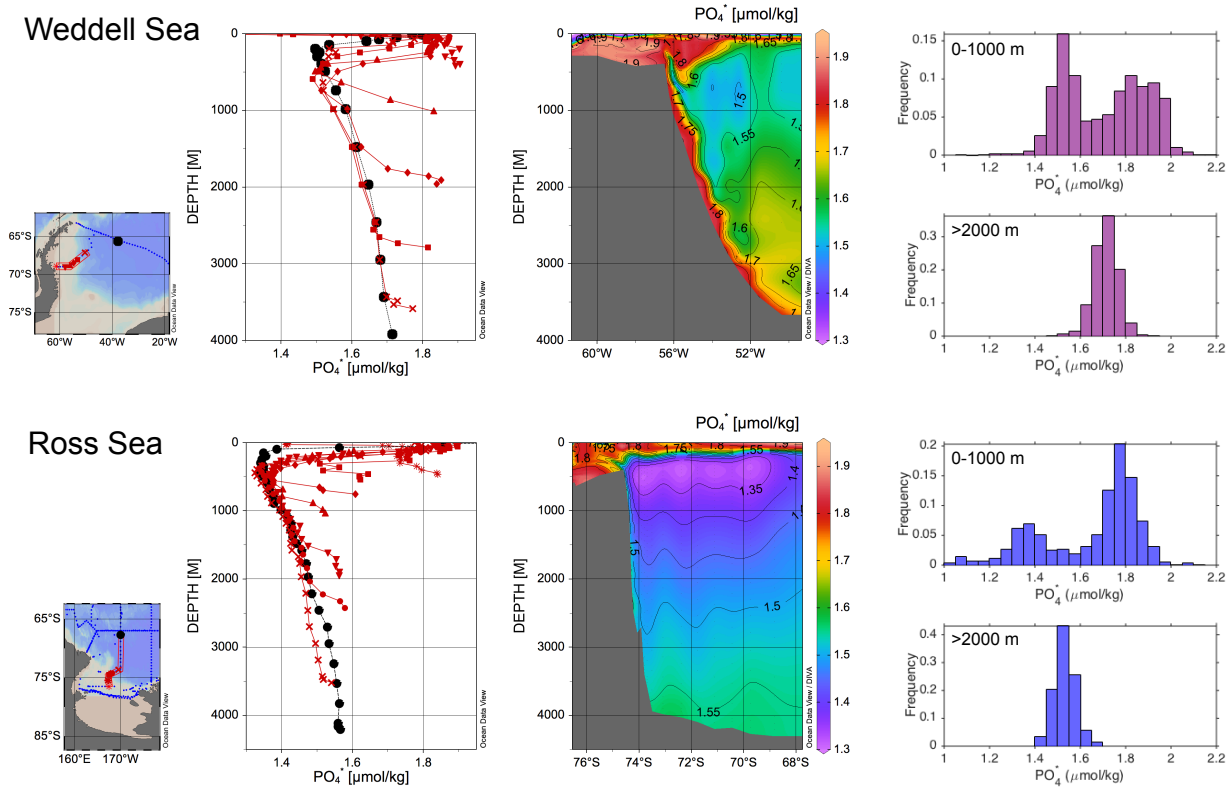

Figure 4: PO_4* data in the Weddell and Ross Seas from the GLODAPv2 database. Sections (central panel) show high PO_4* values on the shelves, that descend the continental margin in a narrow plume (Warren 1981). This is also picked out by selected depth profiles along these sections (left hand panel), with the black dots showing a profile further out from the shelf edge. Entrainment of low PO_4* waters in the subsurface reduces southern deep water PO_4*, from 1.95 on the shelf to ~1.65 at depth. This can also be seen in the histograms in the right hand panel (encompassing larger areas than those shown in the maps and sections), which show two distinct PO_4* populations in the top 1000 m, which mix to give the more homogenous values at depth. Note that Weddell Sea waters have higher PO_4* than Ross Sea waters, likely due to less influence of low-PO_4* NADW and higher local deep water formation rates, elevating PO_4* throughout this more enclosed basin. Data are from GLODAPv2 (Key et al., 2015; Olsen et al., 2016) with profiles, maps, and sections plotted in ODV (Schlitzer 2015), with sections contoured using isopycnic gridding.

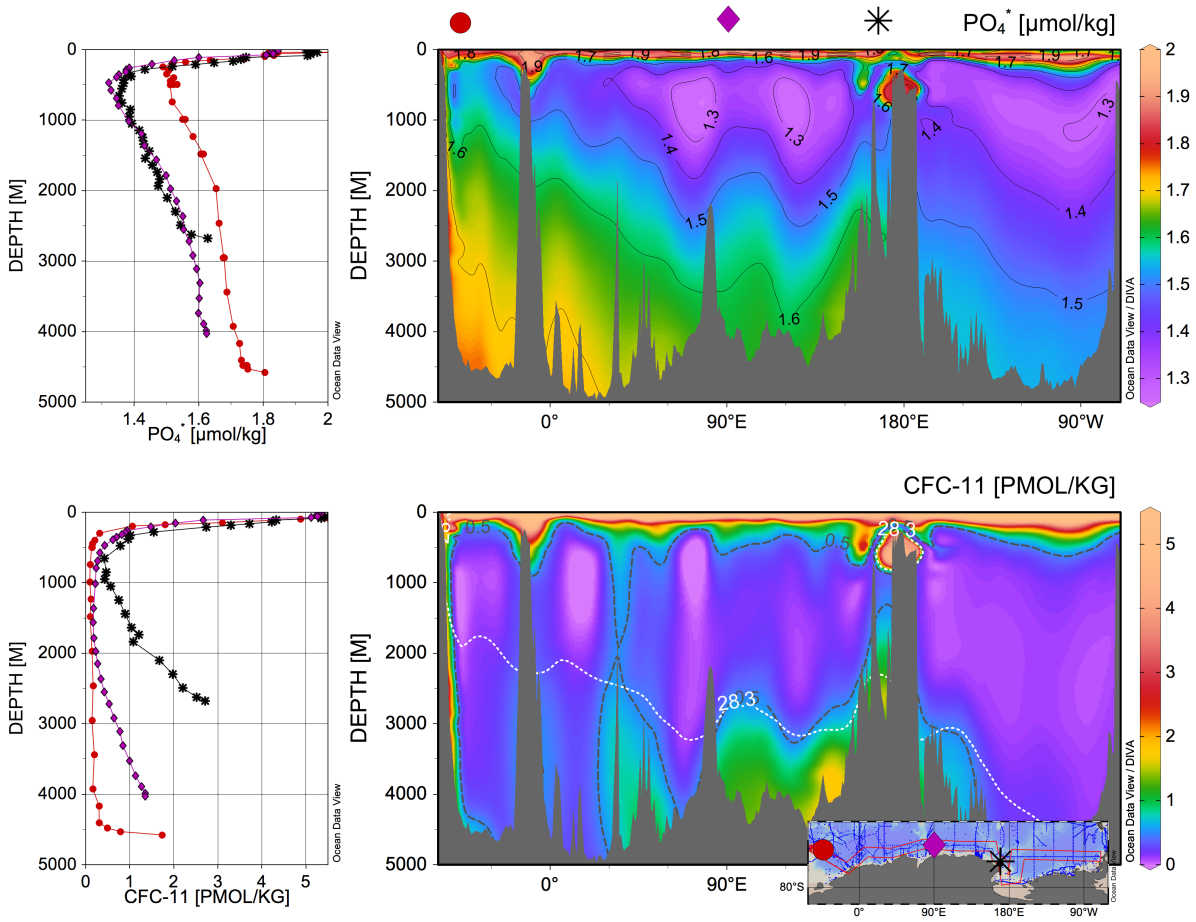

Figure 5. Circum Antarctic sections of PO_4^* and CFC-11 through the southern portion of the Southern Ocean. The locations of the profiles in the left hand panel are illustrated with symbols and shown in the inset map: the red circles are from the Weddell Sea, the purple diamonds from the Antarctic margin in the Indian sector, and the black stars from the northern margin of the Ross Sea. In the CFC section the black dashed line indicates CFC-11 concentrations >0.5 pmol/kg and the white dotted line indicates neutral densities >28.3 kg/m^3; these criteria, along with depth >1500 m, are used to define the alternative deep Southern Ocean PO_4* end member. Data are from GLODAPv2 (Key et al., 2015; Olsen et al., 2016) with profiles, maps, and sections plotted in ODV (Schlitzer 2015), with sections contoured using isopycnic gridding.

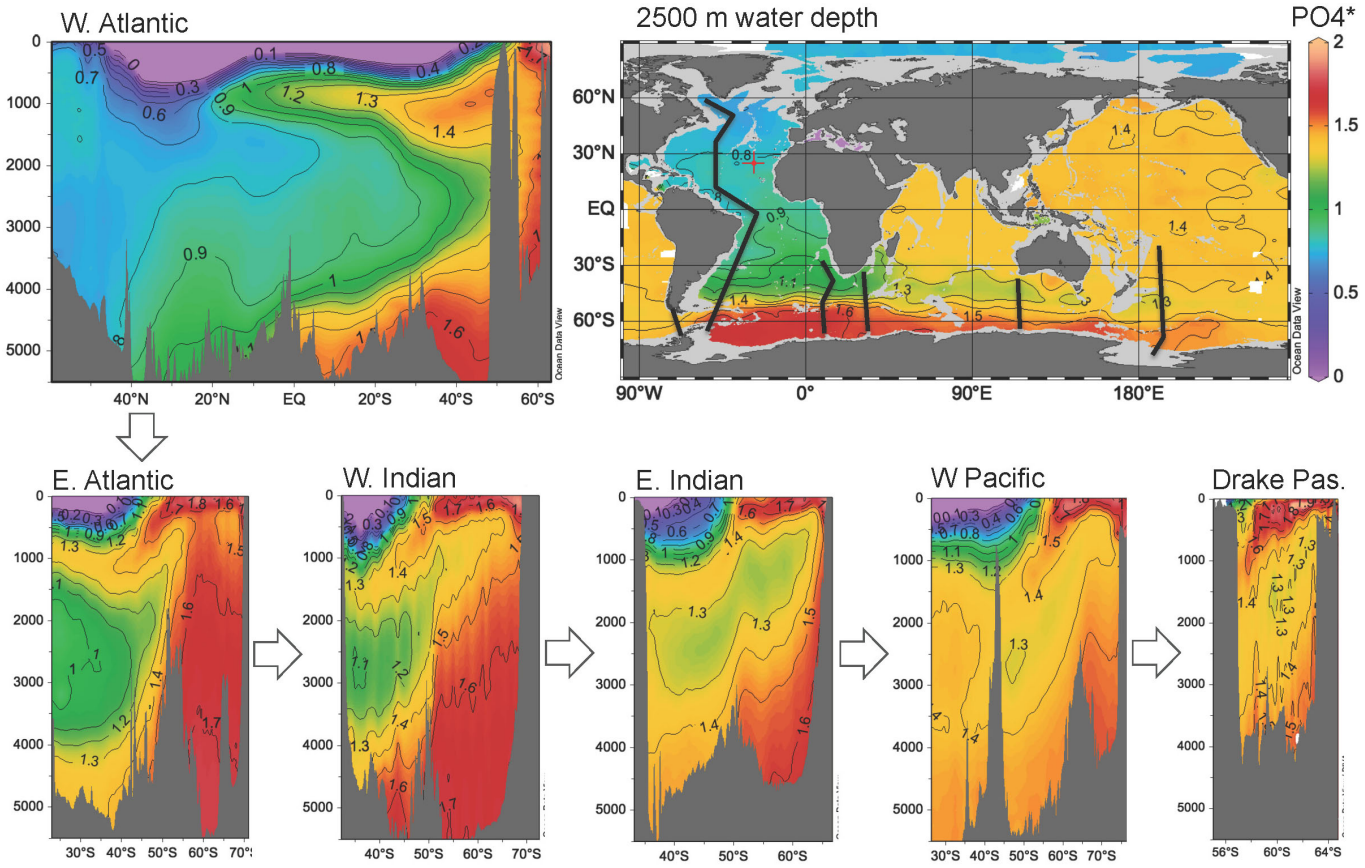

Figure 6. PO_4^* sections for the western Atlantic and for a series of quadrants of the Southern Ocean. Low PO_4^* waters entering the Southern Ocean from the Atlantic and the high PO_4^* waters generated in the Southern Ocean are blended in the Antarctic Circumpolar Current, forming circumpolar deep water. However a PO_4^* high at the seafloor and low at ~2000 m continue to trace the influence of AABW and NADW respectively. Data are from GLODAPv2 (Key et al., 2015; Olsen et al., 2016) with profiles, maps, and sections plotted in ODV (Schlitzer 2015), with sections contoured using isopycnic gridding.

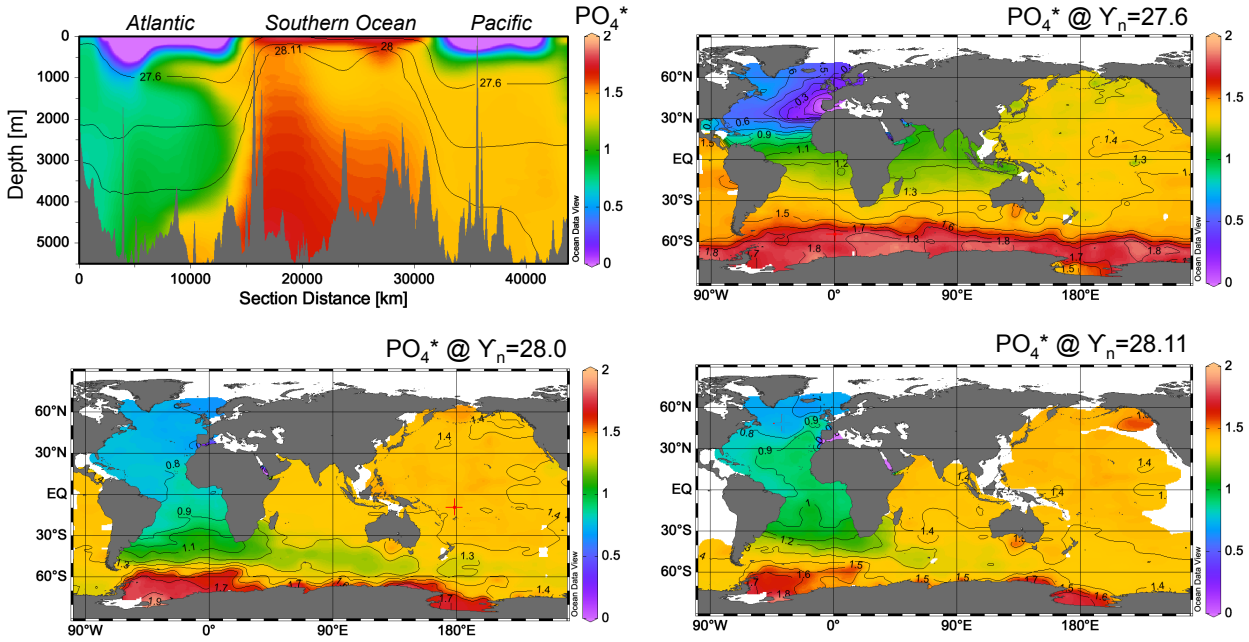

Figure 7. PO_4^* on a section through the Atlantic, Southern, and Pacific Oceans and on the 27.6, 28.0, and 28.11 isopycnal horizons. The depths of these horizons are shown in the section. Mixing of low PO_4^* from the North and high PO_4^* from the South takes place along shared isopycnals, and also diapycnally in the Southern Ocean mixed layer and over rough bottom topography. Data are from GLODAPv2 (Key et al., 2015; Olsen et al., 2016) with profiles, maps, and sections plotted in ODV (Schlitzer 2015).

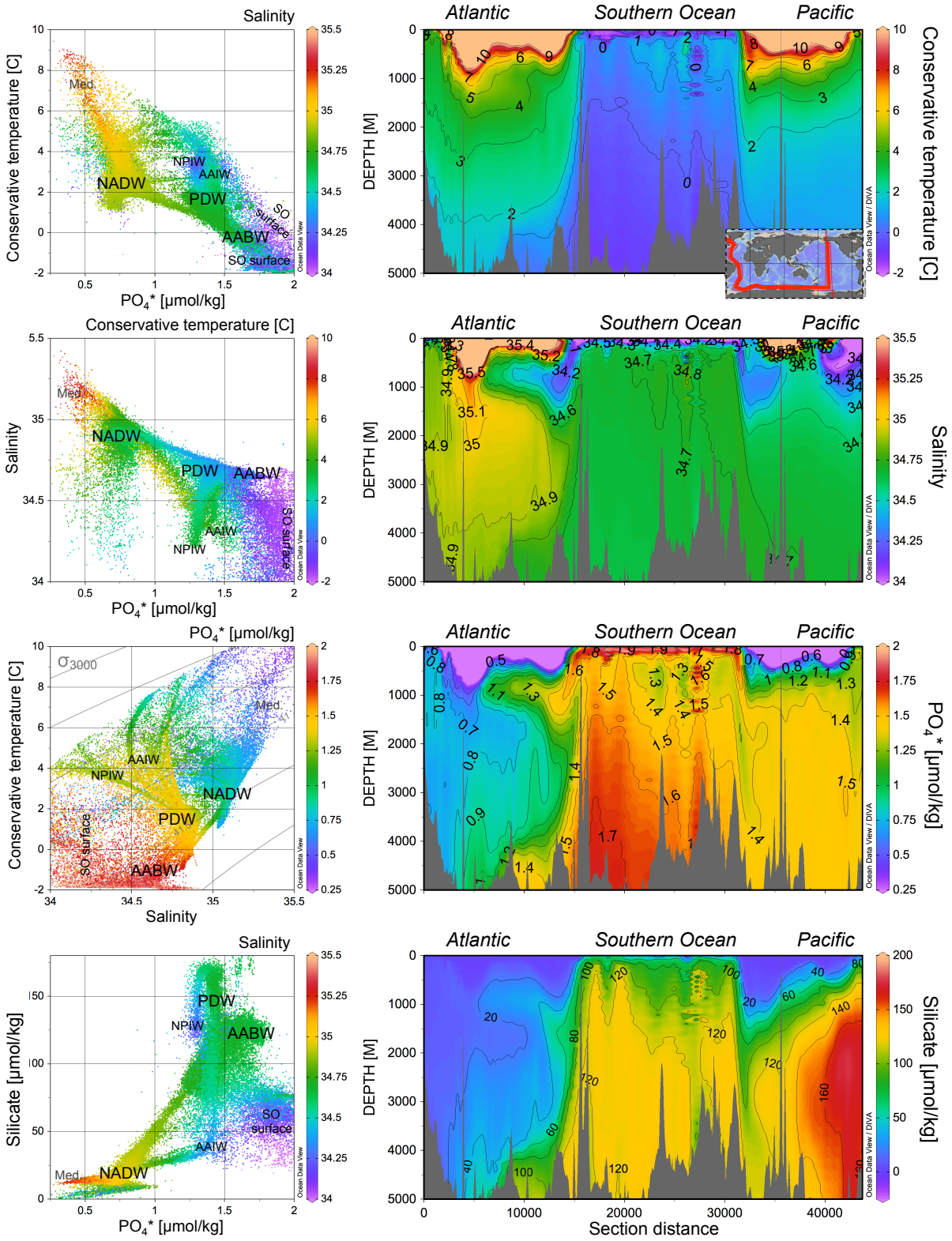

Figure 8: A global hydrographic section for potential temperature, salinity, PO_4*, and silicate. Cross plots show all the data in this section with neutral density greater than 27.2 kg/m^3; the colours of the dots refer to the scale shown to the right of the cross plots. Data are from GLODAPv2 (Key et al., 2015; Olsen et al., 2016) with profiles, maps, and sections plotted in ODV (Schlitzer 2015), with sections contoured using isopycnic gridding.

References

Abernathey, R. and Ferreira, D., 2015. Southern Ocean isopycnal mixing and ventilation changes driven by winds. *Geophysical Research Letters*, *42*(23).

Anderson, L.A. and Sarmiento, J.L., 1994. Redfield ratios of remineralization determined by nutrient data analysis. *Global biogeochemical cycles*, *8*(1), pp.65-80.

Barker, S., Diz, P., Vautravers, M.J., Pike, J., Knorr, G., Hall, I.R. and Broecker, W.S., 2009. Interhemispheric Atlantic seesaw response during the last deglaciation. *Nature*, *457*(7233), pp.1097-1102.

Broecker, W.S., Takahashi, T. and Takahashi, T., 1985. Sources and flow patterns of deep-ocean waters as deduced from potential temperature, salinity, and initial phosphate concentration. *Journal of Geophysical Research: Oceans*, *90*(C4), pp.6925-6939.

Broecker, W.S., Peng, T.H., Ostlund, G. and Stuiver, M., 1985. The distribution of bomb radiocarbon in the ocean. *Journal of Geophysical Research: Oceans*, *90*(C4), pp.6953-6970.

Broecker, W.S., Peacock, S., Walker, S., Weiss, R., Fahrbach, E., Schroeder, M., Mikolajewicz, U., Heinze, C., Carmack, E.C. and Foster, T.D., 1975, November. On the flow of water out of the Weddell Sea. In *Deep Sea Research and Oceanographic Abstracts* (Vol. 22, No. 11, pp. 711-724). Elsevier.

Conkright, M.E., Boyer, T.P. and Levitus, S., 1994. World Ocean Atlas: 1994 Nutrients (Vol. 1). DIANE Publishing.

DeVries, T. and Primeau, F., 2011. Dynamically and observationally constrained estimates of water-mass distributions and ages in the global ocean. Journal of Physical Oceanography, 41(12), pp.2381-2401.

Dong, S., Sprintall, J., Gille, S.T. and Talley, L., 2008. Southern Ocean mixed-layer depth from Argo float profiles. *Journal of Geophysical Research: Oceans*, *113*(C6).

England, M.H., 1995. Using chlorofluorocarbons to assess ocean climate models. *Geophysical Research Letters*, *22*(22), pp.3051-3054.

Ferrari, R., Jansen, M.F., Adkins, J.F., Burke, A., Stewart, A.L. and Thompson, A.F., 2014. Antarctic sea ice control on ocean circulation in present and glacial climates. *Proceedings of the National Academy of Sciences*, *111*(24), pp.8753-8758.

Key, R., Peng, T.-H., Rubin, S. 1998. How much deep water is formed in the Southern Ocean? J. Geophys. Res. 103, 15,833-15,843.

Ganachaud, A. and Wunsch, C., 2000. Improved estimates of global ocean circulation, heat transport and mixing from hydrographic data. *Nature*, *408*(6811), pp.453-457.

Gebbie, G., Huybers, P. 2010. Total matrix intercomparison: A method for determining the geometry of water-mass pathways. J. Phys. Oceanography 40, 1710-1728.

Gordon, A.L. and Huber, B.A., 1990. Southern Ocean winter mixed layer. *Journal of Geophysical Research: Oceans*, *95*(C7), pp.11655-11672.

Gouretski, V. and Koltermann, K.P., 2004. WOCE global hydrographic climatology. *Berichte des BSH*, *35*, pp.1-52.

Hupe, A. and Karstensen, J., 2000. Redfield stoichiometry in Arabian Sea subsurface waters. *Global Biogeochemical Cycles*, *14*(1), pp.357-372.

Johnson, G.C., 2008. Quantifying Antarctic bottom water and North Atlantic deep water volumes. *Journal of Geophysical Research: Oceans*, *113*(C5).

Key, R.M., Olsen, A., van Heuven, S., Lauvset, S.K., Velo, A., Lin, X., Schirnick, C., Kozyr, A., Tanhua, T., Hoppema, M. and Jutterström, S., 2015. Global Ocean Data Analysis Project, Version 2 (GLODAPv2).

Khatiwala, S., Primeau, F., Holzer, M. 2012. Ventilation of the deep ocean constrained with tracer observations and implications for radiocarbon estimates of ideal mean age. Earth Planet. Sci. Lett. 325-326, 116-125.

Lumpkin, R. and Speer, K., 2007. Global ocean meridional overturning. *Journal of Physical Oceanography*, *37*(10), pp.2550-2562.

Maier-Reimer, E. and Hasselmann, K., 1987. Transport and storage of CO 2 in the ocean——an inorganic ocean-circulation carbon cycle model. *Climate dynamics*, *2*(2), pp.63-90.

Marinov, I., Gnanadesikan, A., Toggweiler, J.R. and Sarmiento, J.L., 2006. The southern ocean biogeochemical divide. *Nature*, *441*(7096), pp.964-967.

Marshall, J. and Speer, K., 2012. Closure of the meridional overturning circulation through Southern Ocean upwelling. *Nature Geoscience*, *5*(3), pp.171-180.

Naveira-Garabato, A.C.N., Polzin, K.L., King, B.A., Heywood, K.J. and Visbeck, M., 2004. Widespread intense turbulent mixing in the Southern Ocean. *Science*, *303*(5655), pp.210-213.

Olsen, A., Key, R.M., van Heuven, S., Lauvset, S.K., Velo, A., Lin, X., Schirnick, C., Kozyr, A., Tanhua, T., Hoppema, M. and Jutterström, S., 2016. The Global Ocean Data Analysis Project version 2 (GLODAPv2)–an internally consistent data product for the world ocean. *Earth System Science Data*, *8*(2), p.297.

Orsi, A.H., Johnson, G.C. and Bullister, J.L., 1999. Circulation, mixing, and production of Antarctic Bottom Water. *Progress in Oceanography*, *43*(1), pp.55-109.

Orsi, A.H., Jacobs, S.S., Gordon, A.L. and Visbeck, M., 2001. Cooling and ventilating the abyssal ocean. *Geophysical Research Letters*, *28*(15), pp.2923-2926.

Orsi, A.H., Smethie, W.M. and Bullister, J.L., 2002. On the total input of Antarctic waters to the deep ocean: A preliminary estimate from chlorofluorocarbon measurements. *Journal of Geophysical Research: Oceans*, *107*(C8).

Peacock, S., Visbeck, M. and Broecker, W., 2000. Deep water formation rates inferred from global tracer distributions: An inverse approach. *Inverse Methods in Global Biogeochemical Cycles*, pp.185-195.

Primeau, F., and M. Holzer, 2006: The ocean's memory of the atmosphere: Residence- time and ventilation-rate distributions of water masses. J. Phys. Oceanogr., 36, 1439– 1456.

Roemmich, D., Johnson, G.C., Riser, S., Davis, R., Gilson, J., Owens, W.B., Garzoli, S.L., Schmid, C. and Ignaszewski, M., 2009. The Argo Program: Observing the global ocean with profiling floats. *Oceanography*, *22*(2), pp.34-43.

Sarmiento, J.Á., Gruber, N., Brzezinski, M.A. and Dunne, J.P., 2004. High-latitude controls of thermocline nutrients and low latitude biological productivity. *Nature*, *427*(6969), pp.56-60.

Schlitzer, R., 2007. Assimilation of radiocarbon and chlorofluorocarbon data to constrain deep and bottom water transports in the world ocean. *Journal of Physical Oceanography*, *37*(2), pp.259-276.

Schlitzer, R., Ocean Data View, http://odv.awi.de, 2015.

Schlosser, P., Bonisch, G., Rhein, M. and Bayer, R., 1991. Reduction of Deepwater Formation in the Greenland Sea during the 1980's. *Evidence from Tracer Data, Science*, *251*, p.1054.

Sigman, D.M., Hain, M.P. and Haug, G.H., 2010. The polar ocean and glacial cycles in atmospheric CO2 concentration. *Nature*, *466*(7302), pp.47-55.

Sloyan, B.M. and Rintoul, S.R., 2001. The Southern Ocean limb of the global deep overturning circulation. *Journal of Physical Oceanography*, *31*(1), pp.143-173.

Smethie, W.M. and Fine, R.A., 2001. Rates of North Atlantic Deep Water formation calculated from chlorofluorocarbon inventories. *Deep Sea Research Part I: Oceanographic Research Papers*, *48*(1), pp.189-215.

Stocker, T.F. and Johnsen, S.J., 2003. A minimum thermodynamic model for the bipolar seesaw. *Paleoceanography*, *18*(4).

Takahashi, T., Broecker, W.S. and Langer, S., 1985. Redfield ratio based on chemical data from isopycnal surfaces. *Journal of Geophysical Research: Oceans*, *90*(C4), pp.6907-6924.

Talley, L.D., 1993. Distribution and formation of North Pacific intermediate water. *Journal of Physical Oceanography*, *23*(3), pp.517-537.

Talley, L.D., 1996. Antarctic intermediate water in the South Atlantic. *The South Atlantic: Present and Past Circulation*, pp.219-238.

Talley, L.D., 2013. Closure of the global overturning circulation through the Indian, Pacific, and Southern Oceans: Schematics and transports. *Oceanography*, *26*(1), pp.80-97.

Toggweiler, J.R. and Samuels, B., 1995. Effect of Drake Passage on the global thermohaline circulation. Deep Sea Research Part I: Oceanographic Research Papers, 42(4), pp.477-500.

A. Verdy and M. Mazloff, 2017: A data assimilating model for estimating Southern Ocean biogeochemistry. J. Geophys. Res. Oceans., 122, doi:10.1002/2016JC012650.

Warren, B.A., 1981. Deep circulation of the world ocean. *Evolution of physical oceanography*, pp.6-41.

Appendix Figures

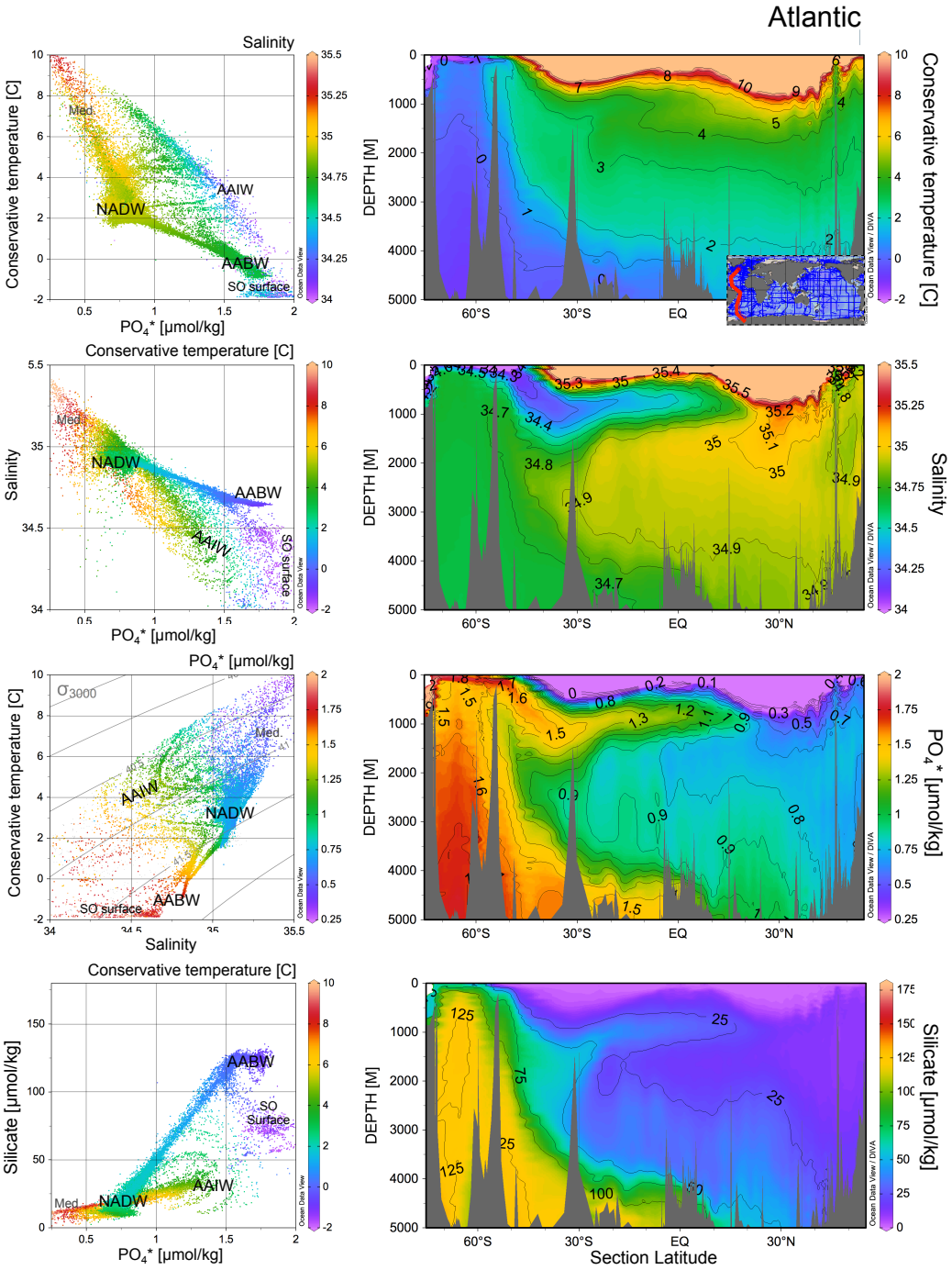

Figure A1: Atlantic hydrographic section for potential temperature, salinity, PO_4*, and silicate. Cross plots show all the data in this section with neutral density greater than 27.2 kg/m^3; the colours of the dots refer to the scale shown to the right of the cross plots. Data are from GLODAPv2 (Key et al., 2015; Olsen et al., 2016) with profiles, maps, and sections plotted in ODV (Schlitzer 2015), with sections contoured using isopycnic gridding.

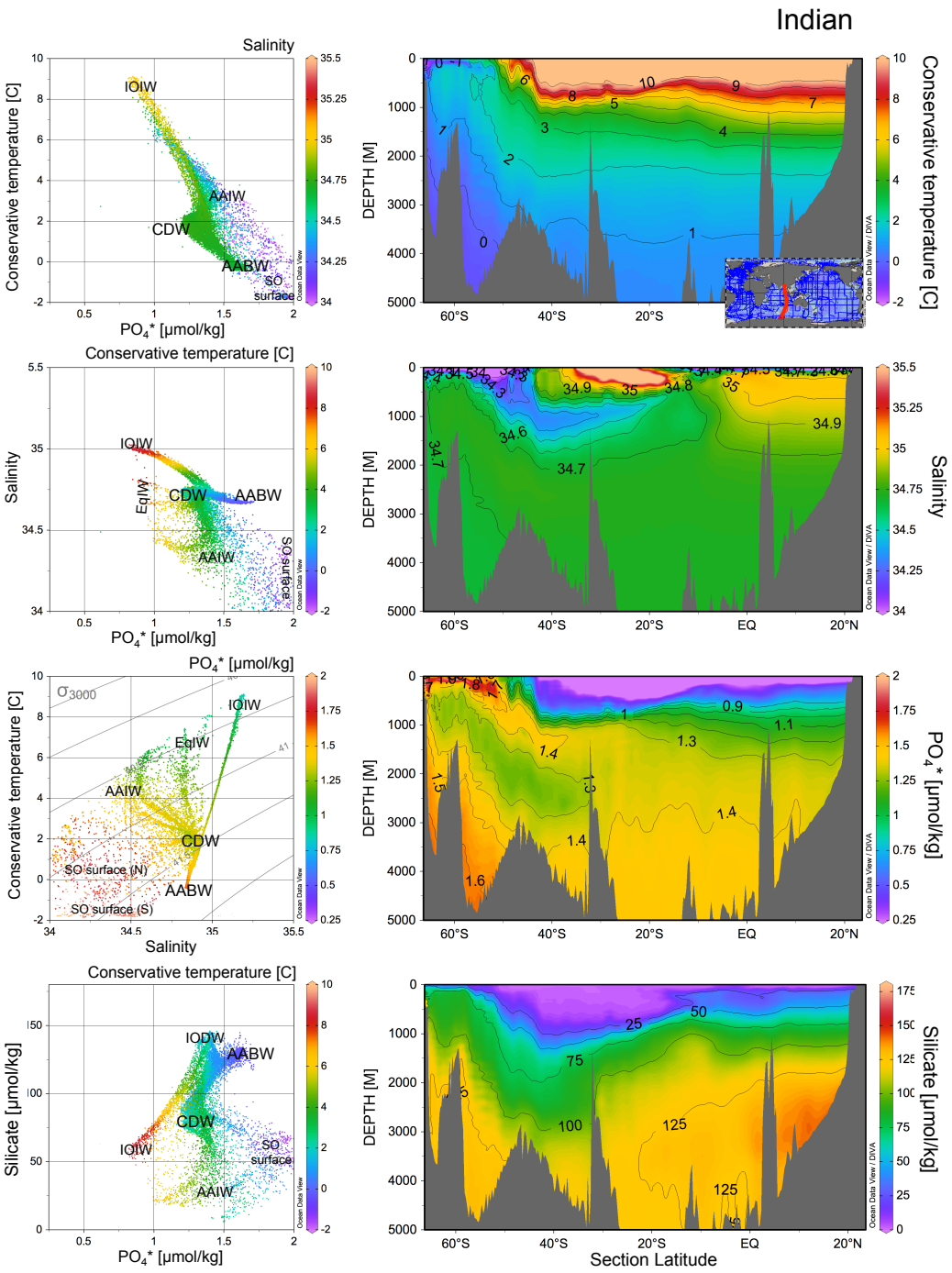

Figure A2: Indian Ocean hydrographic section for potential temperature, salinity, PO_4*, and silicate. Cross plots show all the data in this section with neutral density greater than 27.2 kg/m^3; the colours of the dots refer to the scale shown to the right of the cross plots. Data are from GLODAPv2 (Key et al., 2015; Olsen et al., 2016) with profiles, maps, and sections plotted in ODV (Schlitzer 2015), with sections contoured using isopycnic gridding.

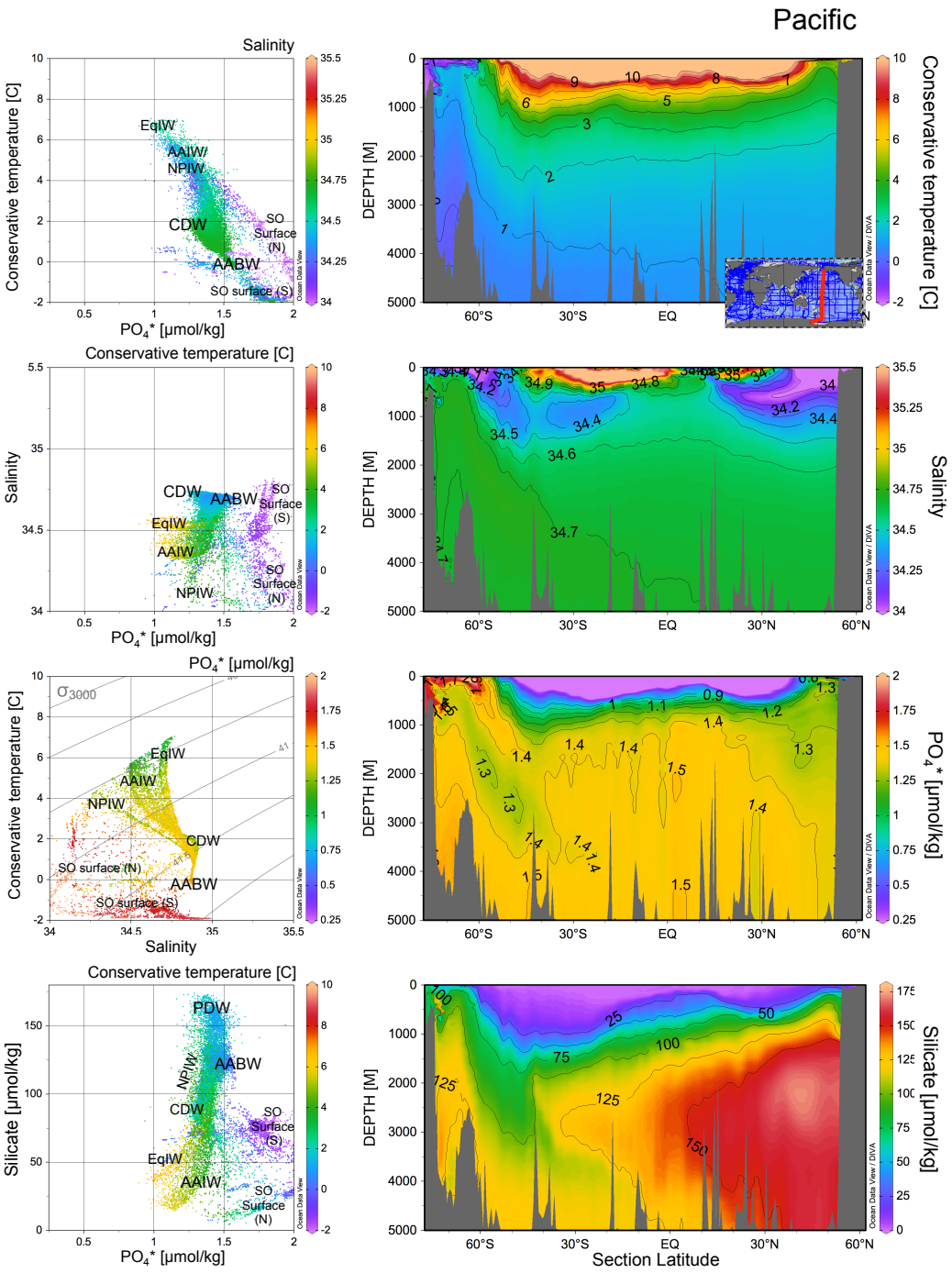

Figure A3: Pacific hydrographic section for potential temperature, salinity, PO_4*, and silicate. Cross plots show all the data in this section with neutral density greater than 27.2 kg/m^3; the colours of the dots refer to the scale shown to the right of the cross plots. Data are from GLODAPv2 (Key et al., 2015; Olsen et al., 2016) with profiles, maps, and sections plotted in ODV (Schlitzer 2015), with sections contoured using isopycnic gridding.

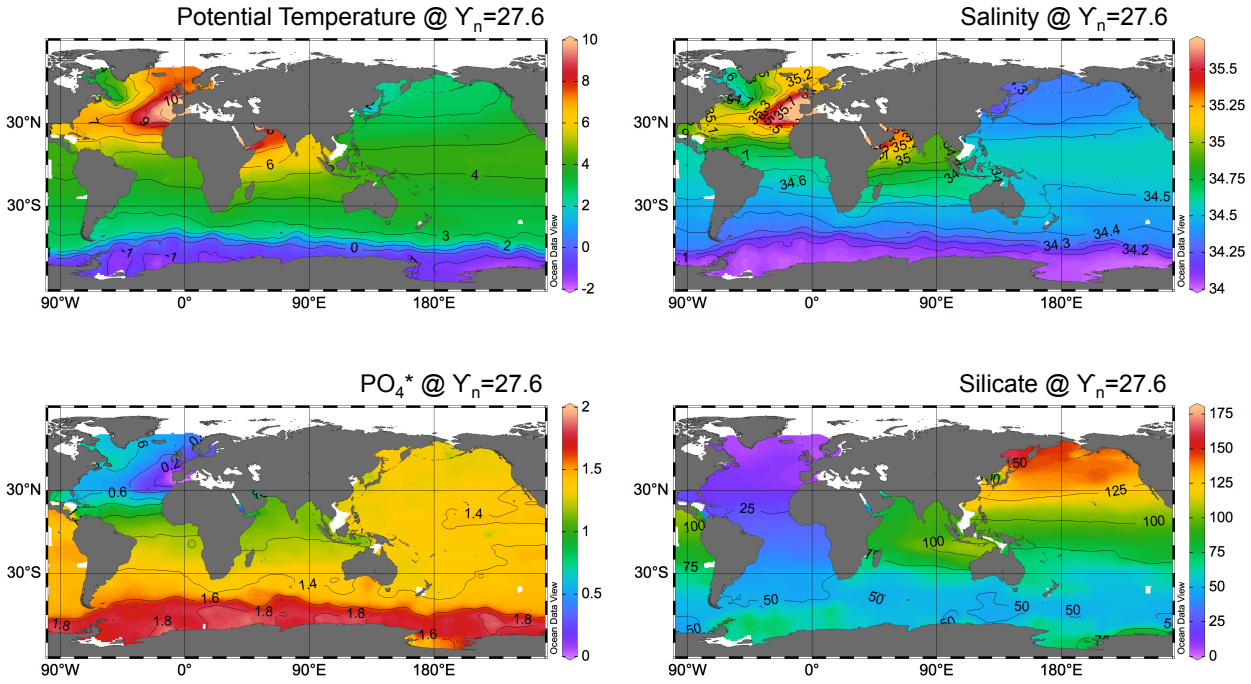

Figure A4: Potential temperature, salinity, PO_4*, and silicate on the 27.6 isopycnal horizon. The depth of this horizon is shown in Figure 8 and averages ~1000 m in the basins and is in the mixed layer in the Southern Ocean. Data are from GLODAPv2 (Key et al., 2015; Olsen et al., 2016) with profiles, maps, and sections plotted in ODV (Schlitzer 2015).

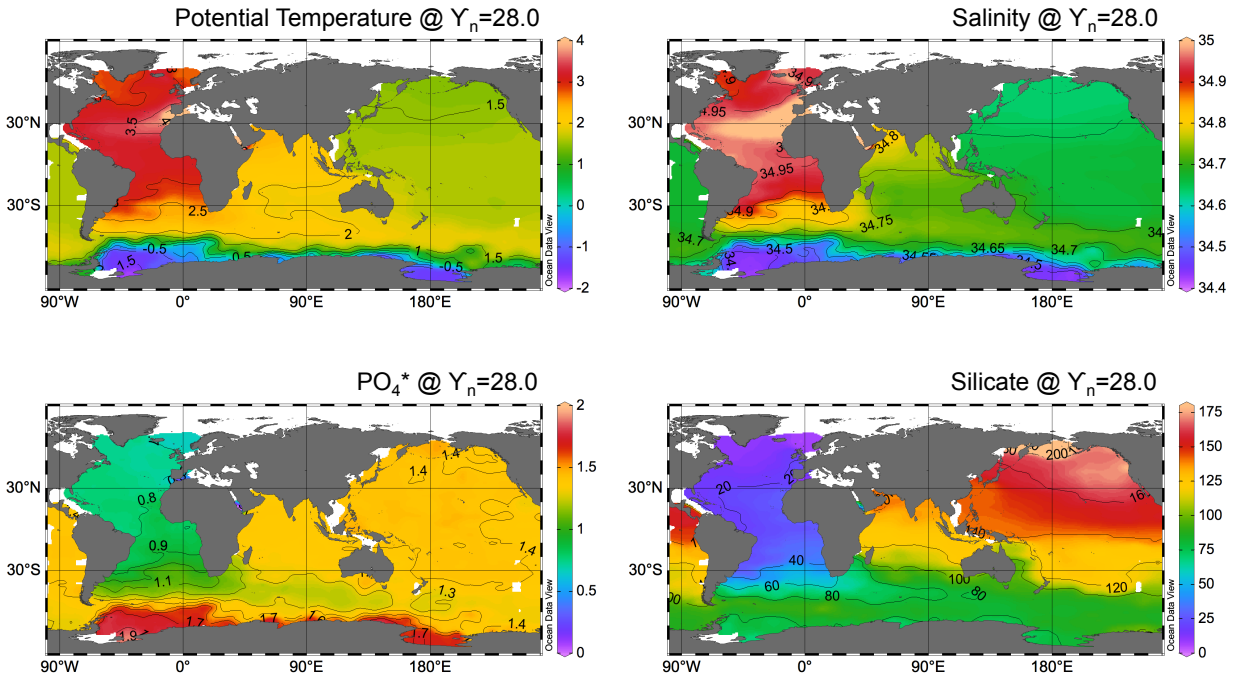

Figure A5: Potential temperature, salinity, PO_4*, and silicate on the 28.0 isopycnal horizon. The depth of this horizon is shown in Figure 8 and averages ~2500 m in the basins and ~250 m in the mixed layer in the Southern Ocean. Data are from GLODAPv2 (Key et al., 2015; Olsen et al., 2016) with profiles, maps, and sections plotted in ODV (Schlitzer 2015).

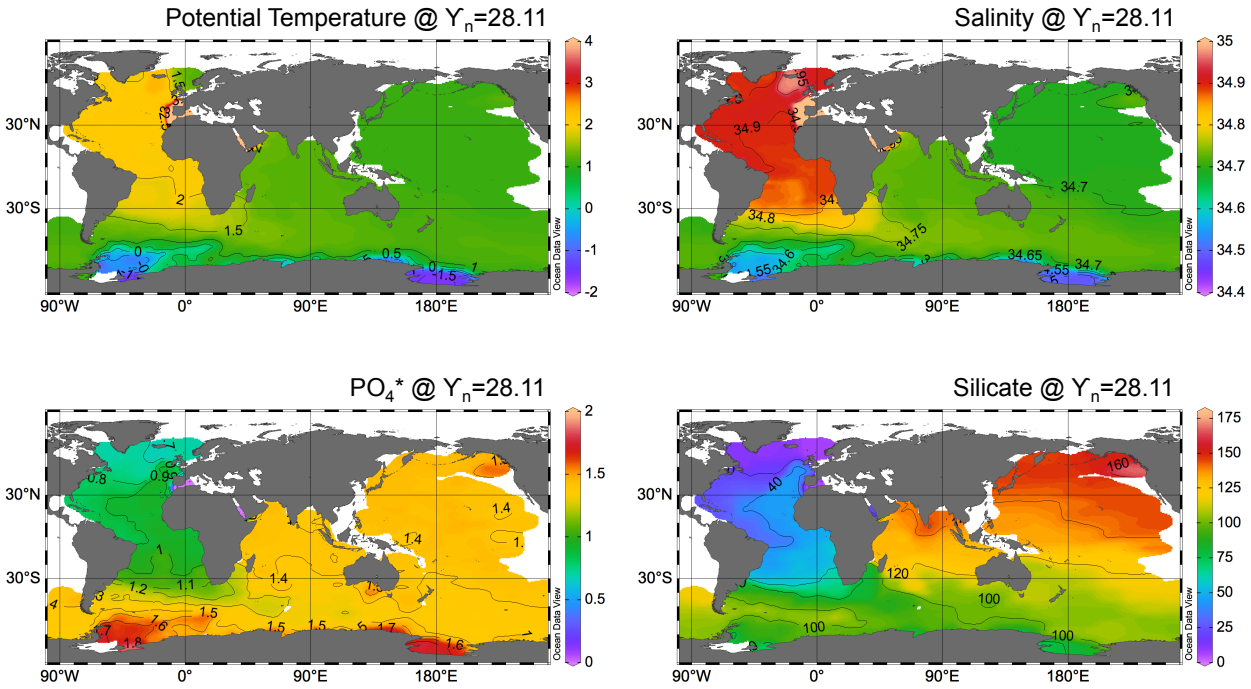

Figure A6: Potential temperature, salinity, PO_4*, and silicate on the 28.3 isopycnal horizon. The depth of this horizon is shown in Figure 8 and averages ~4000 m in the basins and ~400 m in the mixed layer in the Southern Ocean. Data are from GLODAPv2 (Key et al., 2015; Olsen et al., 2016) with profiles, maps, and sections plotted in ODV (Schlitzer 2015).